



Short communication

Preferential intergranular oxidation as a potential degradation mechanism for Alloy X-750 CANDU spacers

A.E. Yaedu^a, L. Volpe^b, J.D. Henderson^c, S. Ramamurthy^c, K. Daub^a, F. Scenini^d, S. Y. Persaud^{a,*}

^a Queen's University, 60 Union Street W, Kingston, ON K7L 2N8, Canada

^b Material Division, United Kingdom Atomic Energy Authority, Culham Campus, Abingdon OX14 3DB, UK

^c Surface Science Western, The University of Western Ontario, London N6G 0J3, Canada

^d Department of Materials and Royce Institute, The University of Manchester, Oxford Road, Manchester M13 9PL, UK



ARTICLE INFO

Keywords:

CANDU spacer

Alloy X-750

Preferential intergranular oxidation

ABSTRACT

Oxidation experiments on Alloy X-750 were performed in reducing CO-CO₂ mixtures to assess the possibility of preferential intergranular oxidation (PIO) in relation to CANDU garter-spring spacers. The testing environments simulate hypothetical off-chemistry scenarios, promoting the oxidation of the alloying elements, but not Ni. Surface and cross-section microscopy corroborated by Auger electron spectroscopy confirmed the occurrence of internal and intergranular oxidation in Alloy X-750, accompanied by Ni nodule expulsion to the surface. Results are qualitatively similar to observations in Alloy 600 exposed to 480°C hydrogenated steam, used as an accelerated environment for primary water stress corrosion cracking (PWSCC) testing.

CANada Deuterium Uranium (CANDU) reactors use garter spring spacers to prevent contact between the hot pressure tube and the colder calandria tubes. Contact must be avoided to reduce the likelihood of Zr hydride formation which can lead to cracking of the fuel-containing pressure tubes [1]. The space between the tubes, designated as annular gas system (AGS), works as an insulating space and as a detection system as it is filled with a recirculating CO₂-O₂ mixture, with its moisture content constantly monitored to detect water ingress [2]. Spacers are made of either a Zr alloy or Alloy X-750 (Ni-16Cr-7Fe-2.5-Ti-1Nb-0.7Al), a γ' precipitation-hardened variant of Alloy 600 (72Ni-16Cr-9Fe) thanks to the addition of Al and Ti.

Ex-service Alloy X-750 spacers were found to suffer from embrittlement in crush tests [1], and several studies have been performed to develop mechanisms for this degradation. Hitherto, the embrittlement is solely attributed to the production of He due to transmutation of Ni, which results in He nanobubble formation at cavities and segregation at sinks, such as grain boundaries and matrix-precipitate interfaces [3–5]. However, both Alloy 600 and X-750 are well-known to be susceptible to primary water stress corrosion cracking (PWSCC) [6–9], specifically due to the reducing environment which may have some broad relevance to the AGS. Currently, the model of internal oxidation, originally proposed by Scott and Le Calvar [10], is the most accepted model for the

occurrence of PWSCC in Alloy 600. The internal oxidation model suggests that SCC occurs in Ni-Fe-Cr alloys when the concentration of the reactive element, chromium, is below the internal-to-external oxide transition threshold concentration. Since the Cr content of Alloy 600 and X-750 is identical, the mechanism behind PWSCC in both alloys is likely the same. The AGS is normally an oxidizing environment due to the addition of 0.5–5.0 vol.% O₂, but a small and constant ingress of primary water occurs [2]. Hence, a transient where oxygen is absent can potentially shift from the normally oxidizing to a reducing environment for Ni, similar to primary water conditions.

In this work, we aim to assess whether a reducing CO-CO₂ dry gas mixture can promote the same preferential intergranular oxidation (PIO) commonly observed in Alloy 600 exposed to 480°C H₂-steam, previously used as an accelerated environment for primary water conditions [11]. The objective is to identify whether X-750 could be susceptible to PIO embrittlement in certain CO-CO₂ transient conditions. Thus, in addition to He nanobubbles, intergranular oxidation may contribute to the observed brittle behaviour of ex-service spacers, especially crack initiation.

Samples of X-750 (Heat n° 275097671) with a nominal thickness of 1.09 mm were supplied by Haynes International with chemical composition (wt. %) of 71.83Ni, 15.42Cr, 8.25Fe, 2.45Ti, 0.96Nb,

* Corresponding author.

E-mail address: suraj.persaud@queensu.ca (S.Y. Persaud).

<https://doi.org/10.1016/j.jnucmat.2024.155007>

Received 21 January 2024; Received in revised form 6 March 2024; Accepted 7 March 2024

Available online 8 March 2024

0022-3115/© 2024 The Author(s). Published by Elsevier B.V. This is an open access article under the CC BY license (<http://creativecommons.org/licenses/by/4.0/>).

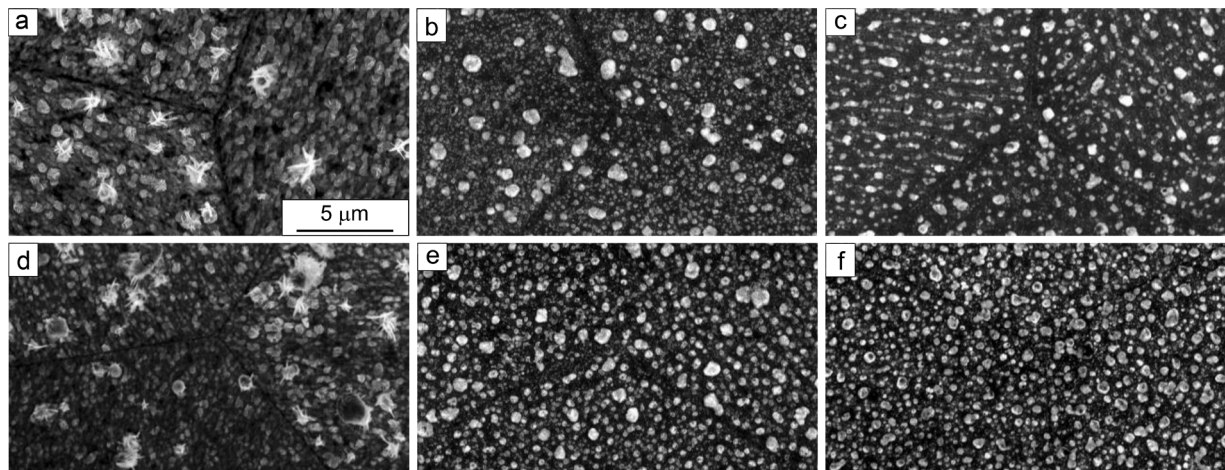


Fig. 1. SE SEM micrographs of aged X-750 tested in the (a) 500 ×, (b) 5,000 × and (c) 100,000 × conditions, and annealed samples tested (d) 500 ×, (e) 5,000 × and (f) 100,000 ×.

0.68Al, 0.23Si, 0.21Mn, 0.05C and 0.01Cu. The samples were prepared in two conditions: solution annealed and thermally aged. These conditions simulate spacer conditions prior to placement in the AGS (aged), and after irradiation (annealed) since the γ' secondary phase is disordered and dissolved by irradiation [3]. Samples with approximate dimensions of $7 \times 7 \text{ mm}^2$ were annealed at $1093 \pm 5^\circ\text{C}$ for one hour in high-purity argon gas, followed by a water quench. Aging was performed at $704 \pm 5^\circ\text{C}$ for 20 h in high-purity argon gas and air-cooled. Note that for in-reactor, spacers are made of a square wire with a cross-section of $0.76 \times 0.76 \text{ mm}^2$ and hot-coiled prior to the HTH heat treatment described above [12]. Afterward, the samples were ground with SiC paper up to 1000 grit, and polished with diamond suspension (6 μm , 3 μm , and 1 μm), finishing with 60 nm colloidal silica. The samples were ultrasonically cleaned with acetone and ethanol for 10 min each and rinsed with deionized water between polishing steps. Each experiment was repeated three times to ensure consistency in results.

The oxidation experiments were performed in a gas reactor similar to the design developed by Scenini et al. [13] where the ratio of several

input gases can be controlled during the test. The gas mixture is directed to a specially designed quartz tube placed inside a furnace. The gas mixture is preheated and mixed in the annular space of the tube before entering the tube and coming in contact with the samples. All experiments were performed at 480°C for 192 h. While 480°C is above the maximum temperature of 330°C experienced by the spacers [14], this temperature allows for accelerated testing and direct comparisons to previous research on Alloy 600 [11,15,16]. From a diffusion kinetics perspective, lattice (bulk) diffusion is essentially negligible at 480°C [16] similar to 330°C , providing an ability for comparison with lower temperature AGS conditions. At the testing temperature of 480°C , the nominal oxygen partial pressure corresponding to the Ni/NiO equilibrium dissociation pressure is $3.12 \times 10^{-24} \text{ bar}$ [17,18]. By changing the ratio of CO to CO_2 , the oxygen partial pressure in the CO- CO_2 mixture was set to the desired reducing condition, defined as the number of times below the NiO oxygen dissociation pressure. In this work, the oxygen partial pressure was set to 500, 5,000, and 100,000 times below the NiO dissociation pressure (designated as 500 ×, 5,000 × and 100,000 ×,

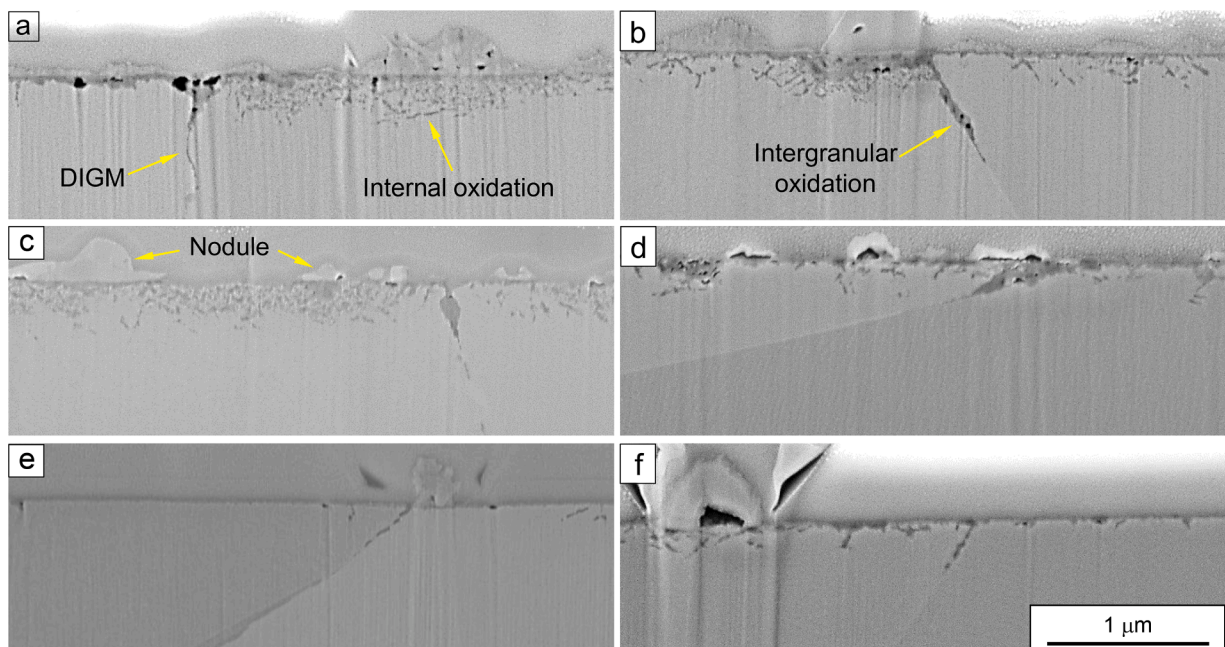


Fig. 2. SEM cross-sectional micrographs from aged X-750 tested at (a) 500 ×, (c) 5,000 × and (e) 100,000 ×; and annealed X-750 samples tested (b) 500 ×, (d) 5,000 × and (f) 100,000 ×. Internal and intergranular oxidation is present in all samples.

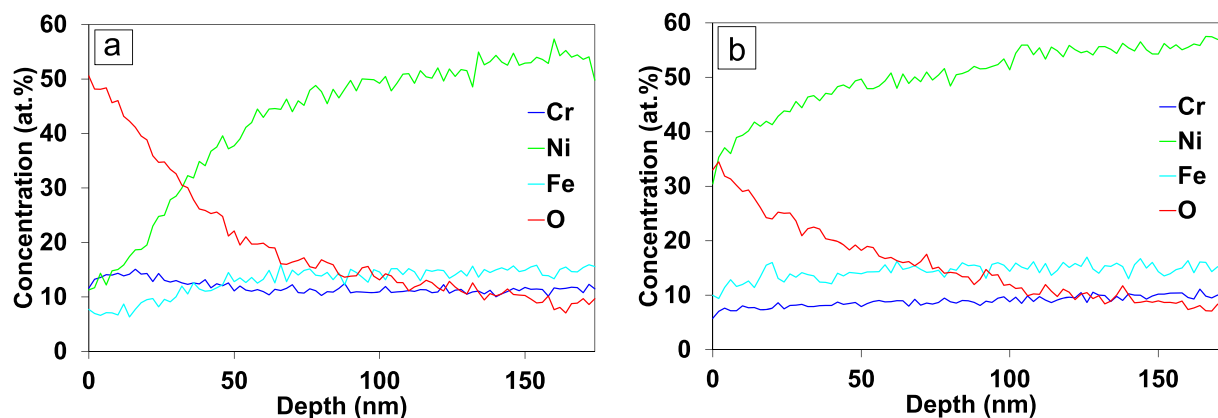


Fig. 3. AES quantitative depth profile taken in an annealed X-750 sample tested in the $5,000\times$ condition and revealing oxygen penetration at both the (a) grain boundary and (b) within the grain.

respectively); thus, the oxygen partial pressure will be not sufficient to oxidize Ni into NiO [19], although Ni-Fe spinel oxides may form.

Post-exposure characterization was performed using scanning electron microscopy (SEM) on a FEI FEG-Nova NanoSEM located at the Reactor Materials Testing Laboratory (RMTL), Queen's University, Kingston, ON, Canada. Micrographs were captured at 10 kV with a working distance of 5 mm. Two site-specific trenches from each sample were prepared to evaluate cross-section oxidation behaviour using a LEO-Zeiss 1540 focused-ion beam (FIB)-SEM located at the Nanofabrication Facility, University of Western Ontario, London, ON, Canada. To confirm whether oxide penetration occurred, Auger electron spectroscopy (AES) was performed with a model 710 field emission scanning Auger nanoprobe located at Surface Science Western, London, ON, Canada. Analyses were performed using 10 keV rastered over the area of interest. Sputtering was performed using 3 keV Ar⁺ ion gun rastered over a $1\times 1\text{ mm}^2$.

Fig. 1 shows secondary electron (SE) micrographs of the X-750 surface after testing. The sample tested at $500\times$ exhibits external oxidation with globular features that resemble nodules found in Alloy 600, Fig. 1a and 1d. However, the globular features have whiskers (or blades) on their surface, which is an indication that they are oxides rather than metallic Ni nodules [20]. This suggests that although the gas environment was thermodynamically reducing for Ni, it was actually oxidizing. This difference may be due to the kinetic limitation of CO oxidation or due to the contaminant oxygen concentration in the gas mixture. On the other hand, the samples tested at $5,000\times$ (Fig. 1b and 1e) and $100,000\times$ (Fig. 1c and 1f) presented a surface with characteristic metallic Ni nodules, which have been previously associated with the formation of internal oxidation for Alloy 600 [21,22]. The formation of metallic Ni nodules on the surface is thought to result from the relief of internal compressive stresses, induced by internal oxidation. This relief occurs through the expulsion of solvent atoms, specifically Ni in this case, to the surface [19]. High-resolution characterization will be performed in future work to characterize internal oxidation and Ni nodule formation. The focus of the present study is intergranular oxidation and the resulting embrittlement.

Following surface analysis, two trenches were milled across grain boundaries in each sample using a FIB-SEM. Fig. 2 shows a cross-sectional image from each of the test conditions, $500\times$, $5000\times$, and $100,000\times$. Close to the surface, darker imaging features are visible along grain boundaries and within the grain, subsequently confirmed by AES to be oxides. These features are strikingly similar in appearance to the intergranular and internal oxidation of Alloy 600 exposed to 480°C H₂-steam [23,24]. Internal oxidation is apparent as small and discrete oxide particles close to the surface, resultant from the oxidation of Fe and Cr. The samples tested at $100,000\times$, Fig. 2e, f, present a significantly diminished internal oxidation in comparison to other testing

conditions due to much lower oxygen content. Intergranular oxidation appears as a dark phase along the grain boundaries close to the surface, with a depth up to approximately $1\ \mu\text{m}$. On the aged sample tested at $500\times$ (Fig. 2a), the grain boundary appears wavy due to diffusion-induced grain boundary migration (DIGM). DIGM is the lateral movement of a grain boundary promoted by the outward diffusion of more reactive alloying elements and is frequently reported in Alloy 600 exposed to 480°C H₂-steam [16,25]. Intergranular carbides are known to hinder intergranular oxide penetration in Alloy 600 [25,26], and Alloy X-750 tested in primary water conditions [8,9]. Distinguishing between carbides and oxides will be explored later in this paper using AES.

The FIB-trench cross-section analysis of the samples tested at $500\times$ corroborates the initial inference that these samples do not exhibit Ni nodules on the surface, Fig. 2a, b. On the other hand, the samples tested at $5,000\times$ and $100,000\times$ (Fig. 2c–f) likely form Ni nodules, similar to reports in Alloy 600 [13,26]. Since aging X-750 promotes the precipitation of carbides along grain boundaries, and the artefacts are too small to be resolved by the conventional energy dispersive spectroscopy (EDX) in the SEM used in this study AES was conducted to confirm the penetration of oxygen along a grain boundary and within a grain. However, it is important to highlight that annealing at 1093°C effectively dissolves nearly all intergranular carbides [27], eliminating the chance of mis-identifying oxides as carbides in the annealed samples. Therefore, the darkly imaged features observed in Fig. 2b, d, f are unlikely to be carbides but more likely to be oxides.

Fig. 3 shows AES quantitative depth profiles taken on an annealed X-750 sample tested at $5,000\times$. A prominent superficial enrichment of oxygen is visible at both the grain boundary (Fig. 3a) and within the grain (Fig. 3b). The concentration of oxygen decreases rapidly while Ni increases up to approximately 100 nm in depth. This indicates oxygen penetration, a result consistent with internal and intergranular oxidation. Although it is not possible to directly correlate the Auger depth profile with a FIB trench image since they were obtained from different grains, the depth profile confirms that the dark features visible in Fig. 2 are associated with internal and intergranular oxides, and not carbide phases. As shown in Fig. 2, the intensity and depth of internal oxidation is variable depending on the testing condition and grain orientation. Intergranular oxidation also exhibits differences, which is likely dependent on material variables, such as grain boundary angle in relation to the surface and the presence or absence of intergranular carbides. As mentioned, experiments with Alloy X-750 in primary water have shown that the presence of intergranular Cr-rich carbides decreases susceptibility to PWSCC. Hence, if the CO-CO₂ environment induces similar behaviour, it is expected that the annealed X-750 samples exhibit more pronounced intergranular oxidation due to the lack of intergranular Cr carbides.

In conclusion, the exposure of Alloy X-750 to CO-CO₂ reducing gas mixtures promotes internal and preferential intergranular oxidation, similar to what observed in Alloy 600 exposed to 480°C H₂-steam. Hence, off-chemistry transients that result in reducing CO-CO₂ dry gas mixtures can, in principle, contribute to the observed embrittlement in Alloy X-750 spacers, especially crack initiation. In other words, intergranular oxidation may produce the initial embrittlement of grain boundaries necessary for crack initiation, with propagation controlled by He nanobubble formation. Future work will further explore internal and intergranular oxidation at the nanoscale using analytical transmission electron microscopy (ATEM) methods. Specifically, the role of Ti, Al, and intergranular carbides in intergranular oxidation will be investigated in detail since studies on Alloy 600 suggest a substantial role of these minor elements in PIO [15,23].

CRedit authorship contribution statement

A.E. Yaedu: Formal analysis, Investigation, Writing – original draft. **L. Volpe:** Methodology, Writing – review & editing. **J.D. Henderson:** Investigation, Writing – review & editing. **S. Ramamurthy:** Investigation, Writing – review & editing. **K. Daub:** Conceptualization, Resources, Methodology, Investigation, Writing – review & editing. **F. Scenini:** Conceptualization, Methodology, Investigation, Writing – review & editing. **S.Y. Persaud:** Conceptualization, Methodology, Investigation, Writing – review & editing, Funding acquisition, Project administration, Supervision.

Declaration of competing interest

The authors declare that they have no known competing financial interests or personal relationships that could have appeared to influence the work reported in this paper.

Data availability

Data will be made available on request.

Acknowledgments

The authors would like to acknowledge the financial support of The University Network of Excellence in Nuclear Engineering (UNENE) and Natural Sciences and Engineering Research Council of Canada (NSERC). The authors are thankful to Haynes International for providing the Alloy X-750 samples employed in this work. The authors would like to thank Dr. Mark Daymond for providing SEM access at the Reactor Materials Testing Laboratory (RMTL) at Queen's University.

References

- [1] M. Griffiths, The effect of irradiation on Ni-containing components in CANDU® reactor cores: a review, *AECL Nucl. Rev.* 2 (1) (2013) 1–16, <https://doi.org/10.12943/ANR.2013.00001>.
- [2] F. R. Greening, "CANDU pressure tube leak detection by annulus gas dew point measurement: a critical review," 2018.
- [3] H.K. Zhang, Z. Yao, C. Judge, M. Griffiths, Microstructural evolution of CANDU spacer material Inconel X-750 under *in situ* ion irradiation, *J. Nucl. Mater.* 443 (1–3) (2013) 49–58, <https://doi.org/10.1016/j.jnucmat.2013.06.034>.
- [4] C.D. Judge, et al., Embrittlement of nickel alloys in a CANDU reactor environment, in: *Proceedings of the 25th Symposium on Effects of Radiation on Nuclear Materials*, ASTM Special Technical Publication, 2013, pp. 161–175, <https://doi.org/10.1520/STP104242>.
- [5] M.N. Tawfeeq, R.J. Klassen, Effect of ion implantation on the grain boundary strength of heat treated Inconel X750, *J. Nucl. Mater.* 516 (2019) 255–263, <https://doi.org/10.1016/j.jnucmat.2019.01.013>.
- [6] J. Blanchet, H. Coriou, L. Grall, C. Mahieu, C. Otter, G. Turluer, Influence de la contrainte, des traitements thermiques et des couplages sur la fissuration intergranulaire des alliages Inconel 600 et X 750, *J. Nucl. Mater.* 55 (2) (1975) 187–206, [https://doi.org/10.1016/0022-3115\(75\)90152-X](https://doi.org/10.1016/0022-3115(75)90152-X).
- [7] P. Skeldon, P. Hurst, Environmentally assisted cracking of Inconel X750, in: *Proceedings of the 3rd International Symposium on Environmental Degradation of Materials in Nuclear Power Systems-Water Reactors*, Traverse City, The Metallurgical Society Inc, 1988, pp. 703–710.
- [8] T. Kekkonen, H. Hänninen, The effect of heat treatment on the microstructure and corrosion resistance of inconel X-750 alloy, *Corros. Sci.* 25 (8–9) (1985) 789–803, [https://doi.org/10.1016/0010-938X\(85\)90011-3](https://doi.org/10.1016/0010-938X(85)90011-3).
- [9] T. Yonezawa, K. Onimura, N. Sakamoto, N. Sasaguri, H. Nakata, H. Susukida, Effect of heat treatment on stress corrosion cracking resistance of high nickel alloys in high temperature water, in: *Proceedings of the International Symposium on Environmental Degradation of Materials in Nuclear Power Systems-Water Reactors*, 1983, pp. 345–367.
- [10] P.M. Scott, M.Le Calvar, Some possible mechanisms of intergranular stress corrosion cracking of alloy 600 in PWR primary water, in: *Proceedings of the 6th International Symposium on Environmental Degradation of Materials in Nuclear Power Systems-Water Reactors*, 1993, pp. 657–667.
- [11] G. Bertali, F. Scenini, M.G. Burke, Advanced microstructural characterization of the intergranular oxidation of Alloy 600, *Corros. Sci.* 100 (2015) 474–483, <https://doi.org/10.1016/j.corsci.2015.08.010>.
- [12] L. Marc, P. Nandu, S. Basma, *The Technology of CANDU Fuel Channels*, AECL, 2012.
- [13] F. Scenini, R.C. Newman, Alloy oxidation studies related to PWSCC, in: *Proceedings of the 12th International Conference on Environmental Degradation of Materials in Nuclear Power Systems - Water Reactors*, 2005, pp. 891–902.
- [14] C.D. Judge, *The Effects of Irradiation on Inconel X-750*, McMaster University, Hamilton, ON, 2015.
- [15] L. Volpe, M.G. Burke, F. Scenini, Correlation between grain boundary migration and stress corrosion cracking of alloy 600 in hydrogenated steam, *Acta Mater.* 186 (2020) 454–466, <https://doi.org/10.1016/j.actamat.2020.01.020>.
- [16] S.Y. Persaud, R.C. Newman, A review of oxidation phenomena in Ni alloys exposed to hydrogenated steam below 500°C, *Corrosion* 72 (7) (2016) 881–896, <https://doi.org/10.5006/1957>. National Assoc. of Corrosion Engineers International.
- [17] S.Y. Persaud, S. Ramamurthy, R.C. Newman, Internal oxidation of alloy 690 in hydrogenated steam, *Corros. Sci.* 90 (2015) 606–613, <https://doi.org/10.1016/j.corsci.2014.11.006>.
- [18] L. Volpe, M. Curioni, M.G. Burke, F. Scenini, Thermodynamic equivalence charts for stress corrosion cracking studies in hydrogenated steam, high pressure and supercritical water, *J. Electrochem. Soc.* 168 (1) (2021) 011501, <https://doi.org/10.1149/1945-7111/abd570>.
- [19] O. Kubaschewski, *Materials Thermochemistry*, 6th ed., Pergamon, New York, 1993.
- [20] P. Kofstad, *High Temperature Oxidation of Metals*, John Wiley & Sons, New York, NY, 1966.
- [21] L. Volpe, M.G. Burke, F. Scenini, Understanding the role of Diffusion Induced Grain Boundary Migration on the preferential intergranular oxidation behaviour of Alloy 600 via advanced microstructural characterization, *Acta Mater.* 175 (2019) 238–249, <https://doi.org/10.1016/j.actamat.2019.06.021>.
- [22] Y. Ghaffari, K. Daub, F. Long, M. Topping, S. Persaud, Comparing the intergranular oxidation of Ni-Cr and Ni-Al model alloys in 480°C hydrogenated steam, *Scr. Mater.* 232 (2023) 115501, <https://doi.org/10.1016/j.scriptamat.2023.115501>.
- [23] G. Bertali, F. Scenini, M.G. Burke, The effect of residual stress on the preferential intergranular oxidation of Alloy 600, *Corros. Sci.* 111 (2016) 494–507, <https://doi.org/10.1016/J.CORSCI.2016.05.022>.
- [24] S.Y. Persaud, et al., Grain boundary embrittlement of alloy 600 by internal oxidation in simulated primary water environments, in: *Proceedings of the 16th International Conference on Environment Degradation of Materials in Nuclear Power Systems - Water Reactors*, 2013.
- [25] G. Bertali, F. Scenini, M.G. Burke, The intergranular oxidation susceptibility of thermally-treated Alloy 600, *Corros. Sci.* 114 (2017) 112–122, <https://doi.org/10.1016/j.corsci.2016.11.004>.
- [26] S.Y. Persaud, A. Korinek, J. Huang, G.A. Botton, R.C. Newman, Internal oxidation of alloy 600 exposed to hydrogenated steam and the beneficial effects of thermal treatment, *Corros. Sci.* 86 (2014) 108–122, <https://doi.org/10.1016/J.CORSCI.2014.04.041>.
- [27] G.P. Sabol, R. Stickler, Microstructure of nickel-based superalloys, *Phys. Status Solidi (B)* 35 (1) (1969) 11–52, <https://doi.org/10.1002/pssb.19690350102>.